

Strain engineering and hydrogen effect for two-dimensional ferroelectricity in monolayer group-IV monochalcogenides MX ($M = \text{Sn, Ge}$; $X = \text{Se, Te, S}$)

Maurice Franck Kenmogne Ndjoko¹, Bi-Dan Guo(郭必诞)², Yin-Hui Peng(彭银辉)², and Yu-Jun Zhao(赵宇军)^{1,2,†}

¹Department of Materials Science and Engineering, South China University of Technology, Guangzhou 510640, China

²Department of Physics, South China University of Technology, Guangzhou 510640, China

(Received 15 March 2022; revised manuscript received 25 May 2022; accepted manuscript online 29 May 2022)

Two-dimensional (2D) ferroelectric compounds are a special class of materials that meet the need for devices miniaturization, which can lead to a wide range of applications. Here, we investigate ferroelectric properties of monolayer group-IV monochalcogenides MX ($M = \text{Sn, Ge}$; $X = \text{Se, Te, S}$) via strain engineering, and their effects with contaminated hydrogen are also discussed. GeSe, GeTe, and GeS do not go through transition up to the compressive strain of -5% , and consequently have good ferroelectric parameters for device applications that can be further improved by applying strain. According to the calculated ferroelectric properties and the band gaps of these materials, we find that their band gap can be adjusted by strain for excellent photovoltaic applications. In addition, we have determined the most stable hydrogen occupancy location in the monolayer SnS and SnTe. It reveals that H prefers to absorb on SnS and SnTe monolayers as molecules rather than atomic H. As a result, hydrogen molecules have little effect on the polarization and electronic structure of monolayer SnTe and SnS.

Keywords: two-dimensional material, strain engineering, ferroelectric photovoltaic materials, hydrogen effect

PACS: 68.35.Gy, 88.40.H-, 73.20.Hb, 77.90.+k

DOI: 10.1088/1674-1056/ac744e

1. Introduction

At certain temperatures, ferroelectric materials could spontaneously exhibit electric polarization. Moreover, the application of an electric field can switch the direction of the polarization. Due to the potential applications of this phenomenon in solar cells, sensors, field-effect transistors, and non-volatile memories, it has attracted tremendous research attention in recent years.^[1–3] To date, however, maintaining ferroelectricity in thin films at room temperature remains a significant challenge.^[4] Some common three-dimensional (3D) ferroelectric materials, for example, PbTiO_3 and BaTiO_3 often lose their ferroelectricity and thus cannot meet the technological demand of the nanoscale devices.^[5] Several attempts have been made at developing two-dimensional (2D) ferroelectric materials to overcome this issue.^[6–9] In response to this, several 2D ferroelectric materials such as graphene and transition metal dichalcogenides,^[10] van der Waals $\text{III}_2\text{–VI}_3$ materials,^[7] group III–IV materials^[3] such as In_2Se_3 ,^[11–13] BiN monolayer,^[14] and SnTe ^[15] have been proposed. 2D materials are considered advantageously due to the large strain engineering of their electronic, magnetic and ferroelectric properties such as in Ga_2S_2 nanoribbons and B_2H_2 layer.^[16,17] However, the spontaneous polarization of some of these ferroelectric 2D materials are relatively low, hence are restricted in their application to certain devices.

Very recently, monolayer group-IV monochalcogenides MX ($M = \text{Ge, Sn}$; $X = \text{S, Se}$), monolayer SbN and mono-

layer BiP thin films were found to be good robustness ferroelectric materials with room temperature less than transition temperature.^[6–8,18–20] The in-plane spontaneous polarization of these monolayers is relatively larger compared to other 2D ferroelectric materials. Moreover, these monolayers have excellent thermoelectric properties as well as massive piezoelectricity.^[21–23] GeSe and SnSe monolayers, on the other hand, were discovered to be promising candidates for the sensing of NO_2 and NH_3 , respectively.^[24,25] The electronic properties of monolayer GeSe were affected by gas molecules impurity on point defects.^[26] Especially, hydrogen is easy to be diffused or pumped to the 2D materials interfaces.^[27,28] However, a thorough understanding of the interaction, particularly the stable configuration of gas molecules in the MX monolayer is still lacking.

In the current study, the first-principle calculations was used to investigate strain engineering ferroelectric properties of group-IV monochalcogenides, and modulate the resulting ferroelectric properties and their band gap. We also explore the effect of Hydrogen impurities on SnS and SnTe monolayer and find out their most stable site, formation energy, and the influence on polarization. The current findings suggest a method for making 2D ferroelectric materials from otherwise designing nanoscale electronic devices and ferroelectric materials.

The following is the structure of the paper. Section 2 describes the computational details, method, and crystal structure, and Section 3 discusses the in-plane ferroelectric polarization in these monolayers MX . Section 4 discusses the strain

[†]Corresponding author. E-mail: zhaoyj@scut.edu.cn

engineering of the ferroelectricity, Section 5 discusses the hydrogen effect on monolayer SnS and SnTe, and Section 6 summarizes our findings.

2. Computational details, method, and the crystal structure

The Vienna *ab initio* simulation package (VASP) was used for the theoretical simulations based on the density functional theory (DFT).^[29,30] The projector augmented wave (PAW) method is used to generate the pseudopotentials.^[31,32] The revised Perdew–Burke–Ernzerhof functional (PBE)^[33] was imposed in the generalized gradient approximation (GGA) exchange and correlation potential since it can describe reasonable structure and electronic properties of crystals. To ensure self-consistency calculations, cutoff energy of 500 eV for plane-wave basis and Γ -centered k -mesh grids $18 \times 18 \times 1$ were used. For total energies during the structural relaxations, the convergence criterion is set to 1 meV. A vacuum layer of 15 Å along the z -direction was allowed to avoid interaction between periodically repeated layers. For ferroelectric polar-

ization calculations, the Berry phase method^[34] is used. We used a (2×2) supercell with 16 atoms to simulate the effects of hydrogen, and the Brillouin zone is integrated using $8 \times 8 \times 1$ Γ -centered k -point mesh.

A typical structure of the monolayer MX ($M = \text{Sn, Ge}$; $X = \text{Se, Te, S}$) is seen in Fig. 1(a). As an example, we consider SnSe, which has a rectangular unit cell with $a = 4.59$ Å and $b = 4.38$ Å and four atoms per cell. Table S1 in the [supporting information](#) contains the lattice parameters for other materials. We use GeSe as an example and set the x -axis as in-plane axes, with the yz -axis parallel to the plane normal. In Fig. 1(a), the dashed orange rectangle represents its non-centrosymmetric unit cell, which contains four atoms and belongs to space group $Pmn21$ with only mirror symmetry. Since the two distinct chemical elements in MX monolayers have appreciable differences in electronegativity and high relative displacement, they are likely to exhibit high spontaneous polarization. To prove the above hypothesis, we require a mechanical strain that can cause in-plane polarization and easily initiate the ferroelectric transition.

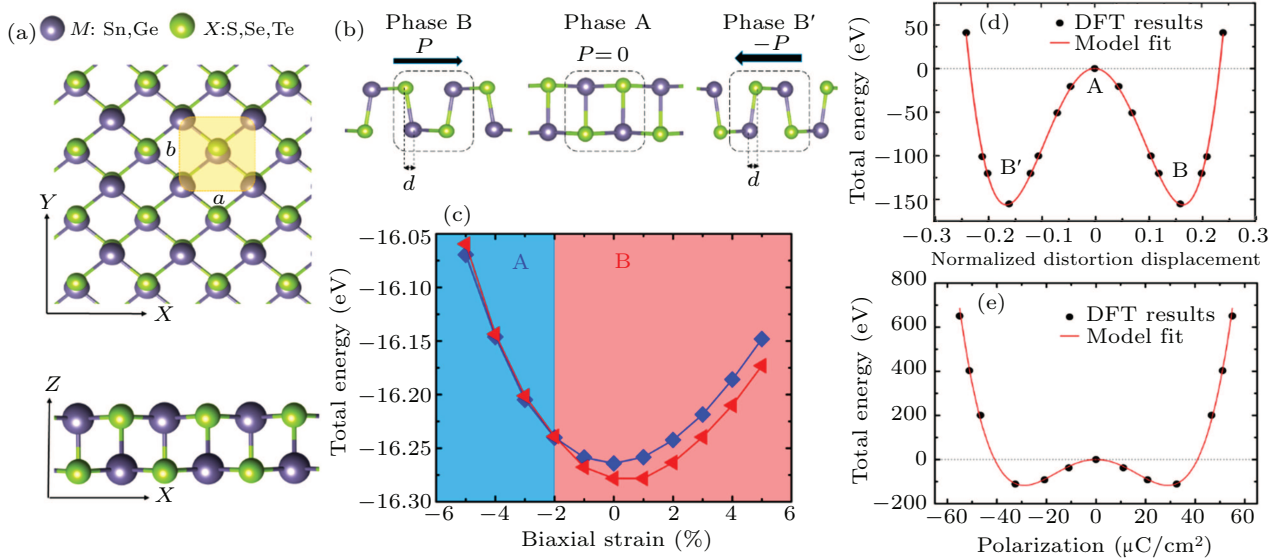


Fig. 1. (a) Top view and side view of monolayer MX structure. The unit cell was dashed by the shaded rectangular region, with a and b being the in-plane lattice constants. (b) Side view of centrosymmetric structure (paraelectric phase A) and two degenerate non-centrosymmetric structures (ferroelectric phase B and B'). (c) Total energy of A and B phases under the biaxial strain of monolayer SnTe, the region where the material represent in-plane polarization is highlighted in light-red. (d) Double-well potential as a function distortion displacement (d) of monolayer GeSe. (e) Double-well potential as a function of spontaneous polarization of monolayer GeS.

Mechanical strain is a powerful tool for modifying the structure characteristics of 2D materials.^[35] We also looked at the structural characteristic of monolayer MX under biaxial tensile strains up to 5%. We have investigated the strain effect on the total energy of monolayer MX in the distorted $Pmn21$ structure (phase B) and the centrosymmetric $Pnma$ structure (phase A) by using a similar structure to bulk MX as shown in Figs. 1(c) and S1, [supporting information](#). We can observe that phase B is stable, and it relaxes spontaneously to phase A. In SnTe, for compressive strains greater than -2% , the non-centrosymmetric B phase becomes more energetically

favourable, denoting the transition from phase B into phase A. However, when the material is subjected to slight strain, the ferroelectric phase can still maintain good stability, which means that monolayer SnTe has good robustness. With the application of biaxial strain, similar trend is found in SnTe and SnS, as demonstrated in Fig. S1, [supporting information](#).

3. In-plane ferroelectric polarization in monolayer MX

The vector d , i.e., the off-center displacement of the Sn atom, was used to quantify the lattice deformation of the crys-

tals, as shown in Fig. 1(b). The centrosymmetric A phase has $d = 0$ and four equal in-plane Sn–Se bonds, which prevents ferroelectricity formation, but the B phase has a nonzero value of displacement and the two covalent Sn–Se bonds are strengthened, causing the inversion symmetry to be broken. The A phase can revert to the energetically degenerated ground state B' phase with opposite displacement upon reversal. As a result, the polarizations of the B and B' phases should be opposing. The lattice parameters are limited to the initial ground state, and the centrosymmetric phase is used as a total energy reference. The pathway through MX monolayers centrosymmetric permits us to determine total polarization by using the Berry phase approach from first-principle DFT calculation^[34] that includes electronic and ionic contributions. The double-well structure in the total energy as a function of polarization is a unique property of spontaneous polarization in a material. The variation in energy of strained monolayer SnSe with respect to normalized distortion displacement and polarization was also determined, and the results are plotted in Figs. 1(d) and 1(e). Figure S2, supporting information, clearly demonstrates double-well potential characteristics. This raises the

possibility of ferroelectric polarization. Spontaneous polarization for GeSe, GeS, SnS, GeTe, SnTe and SnSe monolayer are 36.5, 50.0, 26.5, 33.56, 19.05 and 15.02 $\mu\text{C}/\text{cm}^2$, respectively, equivalence to effective polarization of 35.7, 48.4, 26, 32.8, 19.4 and 18.1 $\mu\text{C}/\text{cm}^2$ in line with recent work.^[8,19] Due to a minimal electronic affinity difference between the type of atoms and, more significantly, the smallest displacement between Sn and Se atoms with respect to the paraelectric state, monolayer SnSe has the least spontaneous polarization.

4. Strain engineering of the ferroelectricity monolayer MX

External strain can have a significant impact on ferroelectricity.^[36] We apply strains using $\epsilon = (a/a_0 - 1)$, where a and a_0 are the strained and unstrained lattice constants along the x - or y -direction to examine the strain modulations of ferroelectricity in monolayer MX . Both biaxial ($\epsilon_x = \epsilon_y$) and uniaxial (ϵ_x) tensile strains can increase the displacement of M atoms relative to the nearby X atoms, thereby increasing the polarization (P_s) values of monolayer MX , as illustrated in Fig. 2.

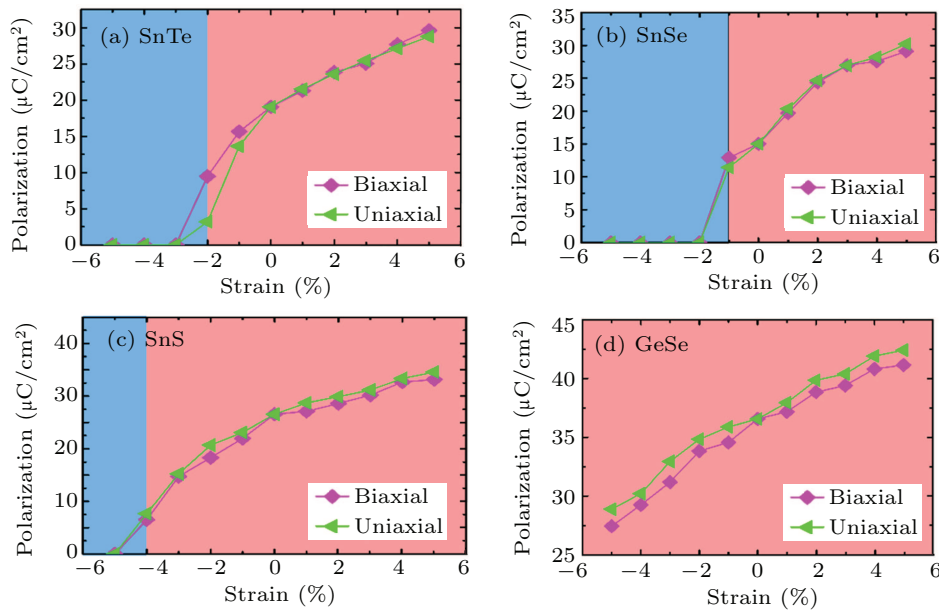


Fig. 2. The evolution of polarization under biaxial and uniaxial strain in (a) SnTe, (b) SnSe, (c) SnS (d) GeSe. The regions of paraelectric and ferroelectric are highlighted by light-blue and light-red, respectively.

As a result, strain engineering may be used to effectively improve the ferroelectricity of monolayer MX . Since the behavior of this ferroelectric transition is based on competition between metastable phases, it is worth looking into how polarization behaves near the transition. When tracing the evolution of P_s in these monolayers MX materials together with the in-plane strain, the amplitude of P_s discontinuously jumps at some critical points. The strain-tuned phase transition occurs in SnTe. This material is paraelectric at the phase transition point of -2% compressive strain. At the biaxial

strain, the in-plane polarization jumps to the transition point value of 3.19% $\mu\text{C}/\text{cm}^2$ for SnTe (Fig. 2(a)). Different situations can be found in 2D SnS and SnSe as illustrated in Figs. 2(b) and 2(c). Biaxial strain (from -5% to 5%) can modulate polarization with a transition point of -1% compressive strain for 2D SnSe, while in 2D SnS transition point occurs up to the compressive strain of value -4% , the value of P_s drops to $6.52 \mu\text{C}/\text{cm}^2$ and increases above the transition point with an increase of strain. In the case of 2D GeSe, GeTe and GeS under strain display the same order of magni-

tude of polarization with highly changed by a larger strain having $P_s = 36.5 \mu\text{C}/\text{cm}^2$, $33.56 \mu\text{C}/\text{cm}^2$, and $50.0 \mu\text{C}/\text{cm}^2$, respectively, without strain, they do not go through ferroelectrics to paraelectric transition up to the compressive strain of -5% . (Figs. 2(d) and S3, supporting information).

To gain a better understanding of the ferroelectric properties of MX materials, the density of states (DOS) of GeSe without strain, is illustrated in Fig. S4, supporting information. It reveals the semiconductor characteristics with a bandgap of about 1.13 eV, in the line with previous report,^[37,38] and is greater than its bulk counterpart, i.e., about 0.68 eV.^[39] Figure 3 illustrates the fluctuation in band gaps of monolayer MX materials as a function of biaxial strain. Traditional ferroelectric photovoltaic materials are widely recognized for having a significant bandgap and hence a relatively low energy conversion. Interestingly, the band gaps of GeSe, SnSe, GeTe, and SnTe in the current investigation are only slightly smaller than the ideal band gap, and they increase as biaxial strain is applied. The bandgap of GeSe with 3.0% strain, in particular, is 1.32 eV, which is the perfect value for photovoltaic applications. Since ferroelectric polarization and an appropriate band gap are two important features in photovoltaic systems, our strain engineering technique in group IV monochalcogenides also enables excellent 2D ferroelectric materials. We expect that our prediction will spur more research on different types of crystals to develop an efficient atomic-scale for ferroelectric photovoltaic devices.

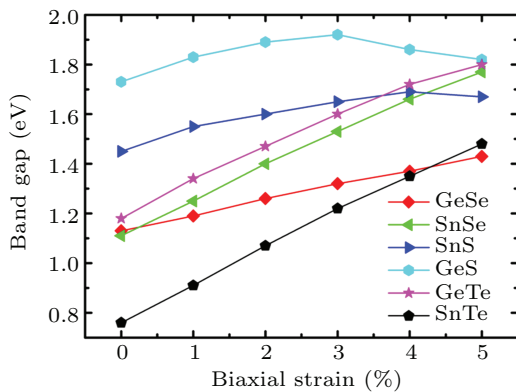


Fig. 3. Band gaps of monolayer MX under biaxial strain.

Properties of ferroelectric materials are highly influenced by inevitable defects, such as hydrogen impurity. In the next part, we focus on the theoretical studies of the impact of hydrogen absorption on ferroelectric polarization stability on monolayer MX .

5. Hydrogen effect on monolayer SnS and SnTe

We have investigated the effect of hydrogen impurity on the electronic structure of monolayer MX using the first-principles calculations. We firstly examine the possible posi-

tions of atomic and molecule H in the SnTe and SnS monolayers. Hydrogen molecule is placed with the H–H vertical or parallel to the surface at the beginning. After verifying several other configurations (Figs. S5 and S6, supporting information), the top and side views of the lowest-energy configurations for H_2 absorbed on monolayer SnTe and SnS are shown in Figs. 4(a) and 4(b). Meanwhile, the atomic H are originally placed at the top and right side between Sn–Te(S) bond as indicated in Figs. S7 and S8, supporting information.

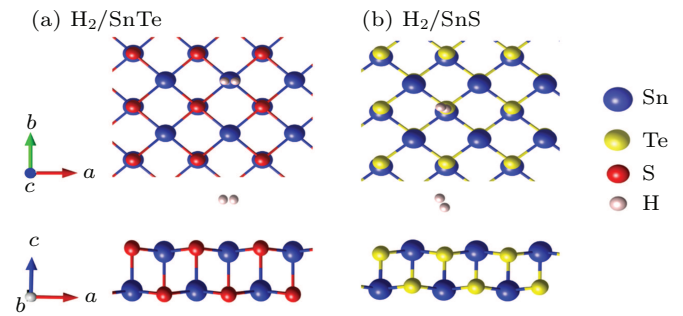


Fig. 4. Top and side views of the relaxed absorbed monolayer with the most favourable configuration for (a) SnTe and (b) SnS.

The formation energy, ΔH_F , calculated to determine the most stable configuration, is defined as $\Delta H_F = E_{2\text{H}+MX} - E_{MX} - \mu(\text{H}_2)$ where $E_{2\text{H}+MX}$, E_{MX} and $\mu(\text{H}_2)$ are the total energies of the two-hydrogen-atom or molecule H_2 adsorbed MX , the pristine MX , and half the hydrogen molecule, respectively. Interestingly, all the hydrogen atoms are relaxed to hydrogen molecules on these monolayers. The most stable absorption configurations of molecule H_2 absorbed on pristine monolayers are shown in Fig. 4. This is in clear contrast from hydrogen in Fe–Ge–Te systems, where atomic hydrogen can be inserted between the layers under gate voltage.^[28] When the SnS and SnTe monolayers are integrated into devices, it is expected that atomic hydrogen could be stabilized by gate voltage as in those Fe–Ge–Te systems. It can be observed that the absorption of the hydrogen molecule introduces a slight distortion to the monolayer of SnTe and SnS, which depend on the binding strength between them. The most stable H molecule adsorption structure is a nearly parallel structure, with the hydrogen molecule pointing toward away or toward the monolayers surface. Based on the most suitable configuration provided above, the following findings for various adsorption systems are achieved.

The calculated formation energies, the equilibrium height, and spontaneous polarization of hydrogen in monolayer SnTe and SnS are listed in Table 1. The negative formation energy denotes that the absorption process is exothermic and energetically favored. The equilibrium height is defined as the nearest two atoms center-to-center distance between the hydrogen molecule and Te or S-layer. It is found that the equilibrium heights of the H molecule binding to the monolayer

SnS is 3.38 Å and SnTe is 3.61 Å, which are greater than the total length of the covalent radii of S and Se atom, respectively. The formation energies of SnS and SnTe are -0.008 eV and -0.01 eV, respectively. Molecule H_2 are physisorbed on SnS and SnTe surfaces, based on the relatively low formation energy and high separation height. Based on the negative and appropriate formation energy values, hydrogen molecule should be a little sensitive to monolayer SnTe and SnS. Insight into the H molecule–monolayer interaction is obtained from spontaneous polarization. The polarization for the pure SnS and SnTe monolayers are found to be $26.57 \mu\text{C}/\text{cm}^2$ and $19.05 \mu\text{C}/\text{cm}^2$, respectively. With the absorption of molecule H_2 , the SnTe and SnS monolayers has no significant changes on the polarization.

Table 1. Calculated formation energies (ΔH_F), equilibrium heights (h), and spontaneous polarization.

Systems	ΔH_F (eV)	h (Å)	P_s ($\mu\text{C}/\text{cm}^2$) with H_2
SnS	-0.008	3.38	19.03
SnTe	-0.01	3.61	26.45

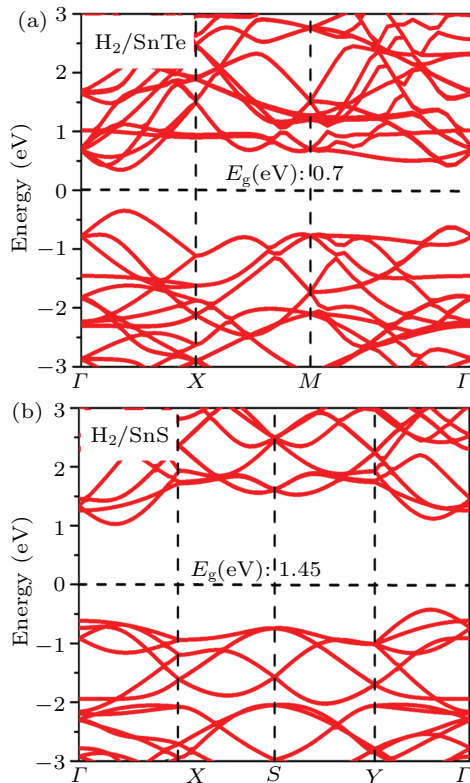


Fig. 5. Band structure of H_2 adsorbed on monolayer (a) SnTe and (b) SnS. The E_g represents the band gap.

The band structures of H_2 -adsorbed monolayer systems are determined to evaluate the impact of H molecule adsorption on the electronic characteristics of monolayer SnS and SnTe as shown in Figs. 5(a) and 5(b). When H_2 are absorbed in the monolayer SnTe and SnS, the band gap of the absorbed system remains the same, i.e., the both valence and conduction bands of the monolayers remain unaltered comparing with the pristine monolayer SnS. In addition, after H molecules are adsorbed, no impurities states are observed in monolayer SnTe

and SnS. As the energy level of 1s in H_2 is about 6 eV below the valence band maximum from our analysis, no impurities states are introduced in the band gap of monolayer SnTe and SnS.

6. Conclusion

In conclusion, based on the first-principles DFT calculation, we proposed a strain engineering approach for generating 2D ferroelectricity in monolayer group-IV monochalcogenides MX ($M = \text{Sn, Ge}$; $X = \text{Se, Te, S}$). The atomic structure and physical characteristics of the materials were investigated. We show that the presence of in-plane ferroelectric polarization in MX monolayers distinguishes them from ferroelectric thin films with out-of-plane polarization, such as perovskite compounds. Moreover, the ferroelectric polarization can increase with an increase of applied tensile strain while compressive strain decreases in all monolayer MX . Our findings also show that the strained GeSe, SnSe, GeTe, and SnTe are promising ferroelectric photovoltaic materials due to their significant ferroelectric polarization and appropriate bandgap.

Furthermore, we study the effect of hydrogen adsorption on monolayer SnS and SnTe. It reveals that hydrogen prefers to physisorb on SnS and SnTe surfaces as molecules, based on the low formation energy and separation height. It introduces no impurity defects in the band gap of the monolayers, and has little impact to their polarization.

Acknowledgements

Project supported by the National Natural Science Foundation of China (NSFC) (Grant No. 12074126), the Foundation for Innovative Research Groups of NSFC (Grant No. 51621001), the Fundamental Research Funds for the Central Universities (Grant No. 2020ZYGXZR076).

References

- [1] Dawber M, Rabe K M and Scott J F 2005 *Rev. Mod. Phys.* **77** 1083
- [2] Scott J F 2007 *Science* **315** 954
- [3] Di Sante D, Stroppa A, Baronne P, Whangbo M H and Picozzi 2015 *Phys. Rev. B* **91** 161401
- [4] Kooi B J and Noheda B 2016 *Science* **353** 221
- [5] Ahn C H, Rabe K M and Triscone J M 2004 *Science* **303** 488
- [6] Chang K, Lin J, Li N H, Wang N, Zhao K, Zhang A, Jin F, Zhong Y, Hu X, Duan W and Zhang Q 2016 *Science* **353** 274
- [7] Ding W J, Zhu J, Wang Z, GaO Y, Xiao D, Gu Y, Zhang Z and Zhu W 2017 *Nat. Commun.* **8** 14956
- [8] Fei R X, Kang W and Yang L 2016 *Phys. Rev. Lett.* **117** 097601
- [9] Wu M H and Zeng X C 2016 *Nano Lett.* **16** 3236
- [10] Li Z W, Hu Y H, Li Y and Fang Z Y 2017 *Chin. Phys. B* **26** 036802
- [11] Ding J, Shao D F, Li M, Wen L and Tsymal E Y 2021 *Phys. Rev. Lett.* **126** 057601
- [12] Soleimani M and Pourfath M 2020 *Nanoscale* **12** 22688
- [13] Xu C, Chen Y, Meingast A, Guo X, Wang F, Lin Z, Lo T W, Maunders C, Lazer S and Wang N 2020 *Phys. Rev. Lett.* **125** 047601
- [14] Zhang X J, Chen P and Liu B G 2017 *J. Mater. Chem. C* **5** 9898
- [15] Xiao C, Wang F, Yang S A, Lu Y, Feng Y and Zhang S 2018 *Adv. Funct. Mater.* **28** 1707383

- [16] Wang B J, Li X H, Zhang L W, Wang G D and Ke S H 2017 *Chin. Phys. B* **26** 057102
- [17] Lei B, Zhang Y Y and Du S X 2019 *Chin. Phys. B* **28** 046803
- [18] Priyadarshi A, Chauhan Y S, Bhowmick S and Agarwal A 2022 *J. Appl. Phys.* **131** 034101
- [19] Wang H and Qian X F 2017 *2D Materials* **4** 015042
- [20] Wan W H, Liu C, Xiao W and Yao Y 2017 *Appl. Phys. Lett.* **111** 132904
- [21] Fei R X and Yang L 2014 *Nano Lett.* **14** 2889
- [22] Peng X H, Wei Q and Copple A 2014 *Phys. Rev. B* **90** 085402
- [23] Priyadarshi A, Chauhan Y S, Bhowmick S and Agarwal A 2018 *Phys. Rev. B* **97** 115434
- [24] Wang J, Yang G F, Xue J J, Lei J M, Chen D J, Lu H, Zhang R and Zheng Y D 2018 *IEEE Electron Device Lett.* **39** 599
- [25] Liu L, Yang Q, Wang Z, Ye H, Chen X, Fan X and Zhang G 2018 *Appl. Surface Sci.* **433** 575
- [26] Mao Y L, Long L, Yuan J, Zhong J and Zhao H 2018 *Chem. Phys. Lett.* **706** 508
- [27] Campbell C T 1997 *Surface Sci. Rep.* **27** 1
- [28] Zheng G L, Xie W Q, Albarakati S, Algarni M, Tan C, Wang Y, Peng J, Partridge J, Farrar L, Yi J and Xiong Y 2020 *Phys. Rev. Lett.* **125** 047202
- [29] Kresse G and Hafner J 1993 *Phys. Rev. B* **47** 13115
- [30] Kresse G and Furthmüller J 1996 *Phys. Rev. B* **54** 11169
- [31] Blöchl P E 1994 *Phys. Rev. B* **50** 17953
- [32] Kresse G and Joubert D 1999 *Phys. Rev. B* **59** 1758
- [33] Perdew J P, Ruzsinsky A, Csonka G I, Vydrov O A, Scuseria G E, Constantin L A, Zhou X and Burke K 2008 *Phys. Rev. Lett.* **100** 136406
- [34] King-Smith R D and Vanderbilt D 1993 *Phys. Rev. B* **47** 1651
- [35] Xu T, Wang X, Mai J, Zhang J and Zhang T Y 2020 *Adv. Electronic Mater.* **6** 1900932
- [36] Haeni J H, Irvin P, Chang W, Uecker R, Reiche P, Li Y L, Choudhury S, Tian W, Hawley M E, Craigo B and Tangantsev 2004 *Nature* **430** 761
- [37] Hu Y H, Zhang S, Sun S, Xie M, Cai B and Zeng H 2015 *Appl. Phys. Lett.* **107** 122107
- [38] Nguyen H T T, Vu T V, Binh N T, Hoat D M, Hieu N V, Anh N T, Nguyen C V, Phuc H V, JapporH R, Obeid M M and Hieu N N 2020 *Chem. Phys.* **529** 110543
- [39] Shin H, Krogel J T, Gasperich K, Kent P R, Benali A and Heinonen O 2021 *Phys. Rev. Mater.* **5** 024002

JUST FOR AUTHORS
— CHINESE PHYSICS B

Chinese Physics B

Volume 32 Number 3 March 2023

Contents

DATA PAPER

- 039801 Measuring stellar populations, dust attenuation and ionized gas at kpc scales in 10010 nearby galaxies using the integral field spectroscopy from MaNGA**
Niu Li and Cheng Li

RAPID COMMUNICATION

- 033102 Transition frequencies between 2S and 2P states of lithium-like ions**
Liming Wang, Tongtong Liu, Weiqing Yang and Zong-Chao Yan
- 034207 Atomic optical spatial mode extractor for vector beams based on polarization-dependent absorption**
Hong Chang, Xin Yang, Jinwen Wang, Yan Ma, Xinqi Yang, Mingtao Cao, Xiaofei Zhang, Hong Gao, Ruifang Dong and Shougang Zhang
- 037305 Superconductivity in epitaxially grown $\text{LaVO}_3/\text{KTaO}_3(111)$ heterostructures**
Yuan Liu, Zhongran Liu, Meng Zhang, Yanqiu Sun, He Tian and Yanwu Xie
- 038103 Reconstruction and functionalization of aerogels by controlling mesoscopic nucleation to greatly enhance macroscopic performance**
Chen-Lu Jiao, Guang-Wei Shao, Yu-Yue Chen and Xiang-Yang Liu

GENERAL

- 030101 Application of the body of revolution finite-element method in a re-entrant cavity for fast and accurate dielectric parameter measurements**
Tianqi Feng, Chengyong Yu, En Li and Yu Shi
- 030201 Inverse stochastic resonance in modular neural network with synaptic plasticity**
Yong-Tao Yu and Xiao-Li Yang
- 030202 Adaptive multi-step piecewise interpolation reproducing kernel method for solving the nonlinear time-fractional partial differential equation arising from financial economics**
Ming-Jing Du, Bao-Jun Sun and Ge Kai
- 030203 An incommensurate fractional discrete macroeconomic system: Bifurcation, chaos, and complexity**
Abderrahmane Abbes, Adel Ouannas and Nabil Shawagfeh
- 030205 Bidirectional visible light absorber based on nanodisk arrays**
Qi Wang, Fei-Fan Zhu, Rui Li, Shi-Jie Zhang and Da-Wei Zhang

(Continued on the Bookbinding Inside Back Cover)

- 030301 Formalism of rotating-wave approximation in high-spin system with quadrupole interaction**
Wen-Kui Ding and Xiao-Guang Wang
- 030302 Floquet scattering through a parity–time symmetric oscillating potential**
Xuzhen Cao, Zhaoxin Liang and Ying Hu
- 030303 High-fidelity universal quantum gates for hybrid systems via the practical photon scattering**
Jun-Wen Luo and Guan-Yu Wang
- 030304 Unified entropy entanglement with tighter constraints on multipartite systems**
Qi Sun, Tao Li, Zhi-Xiang Jin and Deng-Feng Liang
- 030305 Non-Markovianity of an atom in a semi-infinite rectangular waveguide**
Jing Zeng, Yaju Song, Jing Lu and Lan Zhou
- 030306 Performance analysis of quantum key distribution using polarized coherent-states in free-space channel**
Zengte Zheng, Ziyang Chen, Luyu Huang, Xiangyu Wang and Song Yu
- 030307 Security of the traditional quantum key distribution protocols with finite-key lengths**
Bao Feng, Hai-Dong Huang, Yu-Xiang Bian, Wei Jia, Xing-Yu Zhou and Qin Wang
- 030308 Electrical manipulation of a hole ‘spin’–orbit qubit in nanowire quantum dot: The non-trivial magnetic field effects**
Rui Li and Hang Zhang
- 030501 A color image encryption algorithm based on hyperchaotic map and DNA mutation**
Xinyu Gao, Bo Sun, Yinghong Cao, Santo Banerjee and Jun Mou
- 030502 Modulational instability of a resonantly polariton condensate in discrete lattices**
Wei Qi, Xiao-Gang Guo, Liang-Wei Dong and Xiao-Fei Zhang
- 030503 Performance optimization on finite-time quantum Carnot engines and refrigerators based on spin-1/2 systems driven by a squeezed reservoir**
Haoguang Liu, Jizhou He and Jianhui Wang
- 030504 Asymmetric image encryption algorithm based on a new three-dimensional improved logistic chaotic map**
Guo-Dong Ye, Hui-Shan Wu, Xiao-Ling Huang and Syh-Yuan Tan
- 030505 Soliton molecules, T -breather molecules and some interaction solutions in the $(2 + 1)$ -dimensional generalized KDKK equation**
Yiyuan Zhang, Ziqi Liu, Jiaxin Qi and Hongli An
- 030506 All-optical switches based on three-soliton inelastic interaction and its application in optical communication systems**
Shubin Wang, Xin Zhang, Guoli Ma and Daiyin Zhu

030701 Suppression of laser power error in a miniaturized atomic co-magnetometer based on split ratio optimization

Wei-Jia Zhang, Wen-Feng Fan, Shi-Miao Fan and Wei Quan

030702 Fiber cladding dual channel surface plasmon resonance sensor based on S-type fiber

Yong Wei, Xiaoling Zhao, Chunlan Liu, Rui Wang, Tianci Jiang, Lingling Li, Chen Shi, Chunbiao Liu and Dong Zhu

ATOMIC AND MOLECULAR PHYSICS

033101 Ridge regression energy levels calculation of neutral ytterbium ($Z = 70$)

Yushu Yu, Chen Yang and Gang Jiang

033201 Phase-coherence dynamics of frequency-comb emission via high-order harmonic generation in few-cycle pulse trains

Chang-Tong Liang, Jing-Jing Zhang and Peng-Cheng Li

033202 Quantum control of ultrafast magnetic field in H_3^{2+} molecules by tricircular polarized laser pulses

Qing-Yun Xu, Yong-Lin He, Zhi-Jie Yang, Zhi-Xian Lei, Shu-Juan Yan, Xue-Shen Liu and Jing Guo

033401 A theoretical study of fragmentation dynamics of water dimer by proton impact

Zhi-Ping Wang, Xue-Fen Xu, Feng-Shou Zhang and Xu Wang

ELECTROMAGNETISM, OPTICS, ACOUSTICS, HEAT TRANSFER, CLASSICAL MECHANICS, AND FLUID DYNAMICS

034201 Fast population transfer with a superconducting qutrit via non-Hermitian shortcut to adiabaticity

Xin-Ping Dong, Zhi-Bo Feng, Xiao-Jing Lu, Ming Li and Zheng-Yin Zhao

034202 Impact of amplified spontaneous emission noise on the SRS threshold of high-power fiber amplifiers

Wei Liu, Shuai Ren, Pengfei Ma and Pu Zhou

034203 Mid-infrared lightly Er^{3+} -doped CaF_2 laser under acousto-optical modulation

Yuan-Hao Zhao, Meng-Yu Zong, Jia-Hao Dong, Zhen Zhang, Jing-Jing Liu, Jie Liu and Liang-Bi Su

034204 Spectral shift of solid high-order harmonics from different channels in a combined laser field

Dong-Dong Cao, Xue-Fei Pan, Jun Zhang and Xue-Shen Liu

034205 A kind of multiwavelength erbium-doped fiber laser based on Lyot filter

Zhehai Zhou, Jingyi Wu, Kunlong Min, Shuang Zhao and Huiyu Li

034206 Continuous-wave optical enhancement cavity with 30-kW average power

Xing Liu, Xin-Yi Lu, Huan Wang, Li-Xin Yan, Ren-Kai Li, Wen-Hui Huang, Chuan-Xiang Tang, Ronic Chiche and Fabian Zomer

- 034208 Numerical simulation of a truncated cladding negative curvature fiber sensor based on the surface plasmon resonance effect**
Zhichao Zhang, Jinhui Yuan, Shi Qiu, Guiyao Zhou, Xian Zhou, Binbin Yan, Qiang Wu, Kuiru Wang and Xinzhu Sang
- 034209 Anti-symmetric sampled grating quantum cascade laser for mode selection**
Qiangqiang Guo, Jinchuan Zhang, Fengmin Cheng, Ning Zhuo, Shenqiang Zhai, Junqi Liu, Lijun Wang, Shuman Liu and Fengqi Liu
- 034210 Ghost imaging based on the control of light source bandwidth**
Zhao-Qi Liu, Yan-Feng Bai, Xuan-Peng-Fan Zou, Li-Yu Zhou, Qin Fu and Xi-Quan Fu
- 034211 A three-band perfect absorber based on a parallelogram metamaterial slab with monolayer MoS₂**
Wen-Jing Zhang, Qing-Song Liu, Bo Cheng, Ming-Hao Chao, Yun Xu and Guo-Feng Song
- 034212 Giant saturation absorption of tungsten trioxide film prepared based on the seedless layer hydrothermal method**
Xiaoguang Ma, Fangzhen Hu, Xi Chen, Yimeng Wang, Xiaojian Hao, Min Gu and Qiming Zhang
- 034213 A 3–5 μm broadband YBCO high-temperature superconducting photonic crystal**
Gang Liu, Yuanhang Li, Baonan Jia, Yongpan Gao, Lihong Han, Pengfei Lu and Haizhi Song
- 034301 Response characteristics of drill-string guided wave in downhole acoustic telemetry**
Ao-Song Zhao, Hao Chen, Xiao He, Xiu-Ming Wang and Xue-Shen Cao
- 034302 Acoustic propagation uncertainty in internal wave environments using an ocean-acoustic joint model**
Fei Gao, Fanghua Xu, Zhenglin Li, Jixing Qin and Qinya Zhang
- 034303 Tunable topological interface states and resonance states of surface waves based on the shape memory alloy**
Shao-Yong Huo, Long-Chao Yao, Kuan-Hong Hsieh, Chun-Ming Fu, Shih-Chia Chiu, Xiao-Chao Gong and Jian Deng
- 034304 Effect of bio-tissue deformation behavior due to intratumoral injection on magnetic hyperthermia**
Yundong Tang, Jian Zou, Rodolfo C.C. Flesch and Tao Jin
- 034305 Wideband frequency-dependent dielectric properties of rat tissues exposed to low-intensity focused ultrasound in the microwave frequency range**
Xue Wang, Shi-Xie Jiang, Lin Huang, Zi-Hui Chi, Dan Wu and Hua-Bei Jiang
- 034306 Reconfigurable source illusion device for airborne sound using an enclosed adjustable piezoelectric metasurface**
Yi-Fan Tang and Shu-Yu Lin

034501 Resistance law of a rod penetrating a multilayer granular raft

Zonglin Li, Qiang Tian and Haiyan Hu

PHYSICS OF GASES, PLASMAS, AND ELECTRIC DISCHARGES

035201 Intense low-noise terahertz generation by relativistic laser irradiating near-critical-density plasma

Shijie Zhang, Weimin Zhou, Yan Yin, Debin Zou, Na Zhao, Duan Xie and Hongbin Zhuo

CONDENSED MATTER: STRUCTURAL, MECHANICAL, AND THERMAL PROPERTIES

036101 Atomic simulations of primary irradiation damage in U–Mo–Xe system

Wen-Hong Ouyang, Jian-Bo Liu, Wen-Sheng Lai, Jia-Hao Li and Bai-Xin Liu

036402 Investigation of spatial structure and sympathetic cooling in the ${}^9\text{Be}^{+}$ – ${}^{40}\text{Ca}^{+}$ bi-component Coulomb crystals

Min Li, Yong Zhang, Qian-Yu Zhang, Wen-Li Bai, Sheng-Guo He, Wen-Cui Peng and Xin Tong

036801 Atomistic insights into early stage corrosion of bcc Fe surfaces in oxygen dissolved liquid lead-bismuth eutectic (LBE-O)

Ting Zhou, Xing Gao, Zhiwei Ma, Hailong Chang, Tielong Shen, Minghuan Cui and Zhiguang Wang

036802 Strain engineering and hydrogen effect for two-dimensional ferroelectricity in monolayer group-IV monochalcogenides MX ($M = \text{Sn}, \text{Ge}$; $X = \text{Se}, \text{Te}, \text{S}$)

Maurice Franck Kenmogne Ndjoko, Bi-Dan Guo, Yin-Hui Peng and Yu-Jun Zhao

036803 Rational design of Fe/Co-based diatomic catalysts for Li–S batteries by first-principles calculations

Xiaoya Zhang, Yingjie Cheng, Chunyu Zhao, Jingwan Gao, Dongxiao Kan, Yizhan Wang, Duo Qi and Yingjin Wei

036804 Coexisting lattice contractions and expansions with decreasing thicknesses of Cu (100) nano-films

Simin An, Xingyu Gao, Xian Zhang, Xin Chen, Jiawei Xian, Yu Liu, Bo Sun, Haifeng Liu and Haifeng Song

CONDENSED MATTER: ELECTRONIC STRUCTURE, ELECTRICAL, MAGNETIC, AND OPTICAL PROPERTIES

037101 Coexistence of giant Rashba spin splitting and quantum spin Hall effect in H–Pb–F

Wenming Xue, Jin Li, Chaoyu He, Tao Ouyang, Xiongying Dai and Jianxin Zhong

037102 Plasmonic hybridization properties in polyenes octatetraene molecules based on theoretical computation

Nan Gao, Guodong Zhu, Yingzhou Huang and Yurui Fang

- 037103 Prediction of one-dimensional CrN nanostructure as a promising ferromagnetic half-metal**
Wenyu Xiang, Yaping Wang, Weixiao Ji, Wenjie Hou, Shengshi Li and Peiji Wang
- 037104 High-temperature ferromagnetism and strong π -conjugation feature in two-dimensional manganese tetranitride**
Ming Yan, Zhi-Yuan Xie and Miao Gao
- 037201 Reverse gate leakage mechanism of AlGaIn/GaN HEMTs with Au-free gate**
Xin Jiang, Chen-Hao Li, Shuo-Xiong Yang, Jia-Hao Liang, Long-Kun Lai, Qing-Yang Dong, Wei Huang, Xin-Yu Liu and Wei-Jun Luo
- 037202 Quantitative measurement of the charge carrier concentration using dielectric force microscopy**
Junqi Lai, Bowen Chen, Zhiwei Xing, Xuefei Li, Shulong Lu, Qi Chen and Liwei Chen
- 037301 Spin- and valley-polarized Goos-Hänchen-like shift in ferromagnetic mass graphene junction with circularly polarized light**
Mei-Rong Liu, Zheng-Fang Liu, Ruo-Long Zhang, Xian-Bo Xiao and Qing-Ping Wu
- 037302 Design and research of normally-off β -Ga₂O₃/4H-SiC heterojunction field effect transistor**
Meixia Cheng, Suzhen Luan, Hailin Wang and Renxu Jia
- 037303 Low-resistance ohmic contacts on InAlN/GaN heterostructures with MOCVD-regrown n⁺-InGaIn and mask-free regrowth process**
Jingshu Guo, Jiejie Zhu, Siyu Liu, Jielong Liu, Jiahao Xu, Weiwei Chen, Yuwei Zhou, Xu Zhao, Minhan Mi, Mei Yang, Xiaohua Ma and Yue Hao
- 037304 Thermoelectric signature of Majorana zero modes in a T-typed double-quantum-dot structure**
Cong Wang and Xiao-Qi Wang
- 037306 Single-layer intrinsic 2H-phase LuX₂ (X = Cl, Br, I) with large valley polarization and anomalous valley Hall effect**
Chun-Sheng Hu, Yun-Jing Wu, Yuan-Shuo Liu, Shuai Fu, Xiao-Ning Cui, Yi-Hao Wang and Chang-Wen Zhang
- 037401 Abnormal magnetoresistance effect in the Nb/Si superconductor-semiconductor heterojunction**
Zhi-Wei Hu and Xiang-Gang Qiu
- 037402 Flux pinning evolution in multilayer Pb/Ge/Pb/Ge/Pb superconducting systems**
Li-Xin Gao, Xiao-Ke Zhang, An-Lei Zhang, Qi-Ling Xiao, Fei Chen and Jun-Yi Ge
- 037403 Vortex bound states influenced by the Fermi surface anisotropy**
Delong Fang

037501 **Li₂NiSe₂: A new-type intrinsic two-dimensional ferromagnetic semiconductor above 200 K**

Li-Man Xiao, Huan-Cheng Yang and Zhong-Yi Lu

037502 **Orbital torque of Cr-induced magnetization switching in perpendicularly magnetized Pt/Co/Pt/Cr heterostructures**

Hongfei Xie, Yuhan Chang, Xi Guo, Jianrong Zhang, Baoshan Cui, Yalu Zuo and Li Xi

037503 **Enhanced and tunable Imbert–Fedorov shift based on epsilon-near-zero response of Weyl semimetal**

Ji-Peng Wu, Yuan-Jiang Xiang and Xiao-Yu Dai

037504 **Structural evolution-enabled BiFeO₃ modulated by strontium doping with enhanced dielectric, optical and superparamagnetic properties by a modified sol-gel method**

Sharon V S, Veena Gopalan E and Malini K A

037601 **Spin pumping by higher-order dipole-exchange spin-wave modes**

Peng Wang

037701 **Ferroelectricity induced by the absorption of water molecules on double helix SnIP**

Dan Liu, Ran Wei, Lin Han, Chen Zhu and Shuai Dong

037801 **Atomic-scale insights of indium segregation and its suppression by GaAs insertion layer in InGaAs/AlGaAs multiple quantum wells**

Shu-Fang Ma, Lei Li, Qing-Bo Kong, Yang Xu, Qing-Ming Liu, Shuai Zhang, Xi-Shu Zhang, Bin Han, Bo-Cang Qiu, Bing-She Xu and Xiao-Dong Hao

037802 **Crystal and electronic structure of a quasi-two-dimensional semiconductor Mg₃Si₂Te₆**

Chaoxin Huang, Benyuan Cheng, Yunwei Zhang, Long Jiang, Lisi Li, Mengwu Huo, Hui Liu, Xing Huang, Feixiang Liang, Lan Chen, Hualei Sun and Meng Wang

INTERDISCIPLINARY PHYSICS AND RELATED AREAS OF SCIENCE AND TECHNOLOGY

038101 **Suppression and compensation effect of oxygen on the behavior of heavily boron-doped diamond films**

Li-Cai Hao, Zi-Ang Chen, Dong-Yang Liu, Wei-Kang Zhao, Ming Zhang, Kun Tang, Shun-Ming Zhu, Jian-Dong Ye, Rong Zhang, You-Dou Zheng and Shu-Lin Gu

038102 **Tuning the particle size, physical properties, and photocatalytic activity of Ag₃PO₄ materials by changing the Ag⁺/PO₄³⁻ ratio**

Hung N M, Oanh L T M, Chung D P, Thang D V, Mai V T, Hang L T and Minh N V

038401 **Observation of size-dependent boundary effects in non-Hermitian electric circuits**

Luhong Su, Cui-Xian Guo, Yongliang Wang, Li Li, Xinhui Ruan, Yanjing Du, Shu Chen and Dongning Zheng

- 038501 High performance carrier stored trench bipolar transistor with dual shielding structure**
Jin-Ping Zhang, Hao-Nan Deng, Rong-Rong Zhu, Ze-Hong Li and Bo Zhang
- 038502 Analysis of high-temperature performance of 4H-SiC avalanche photodiodes in both linear and Geiger modes**
Xing-Ye Zhou, Yuan-Jie Lv, Hong-Yu Guo, Guo-Dong Gu, Yuan-Gang Wang, Shi-Xiong Liang, Ai-Min Bu and Zhi-Hong Feng
- 038503 High-performance extended short-wavelength infrared PBn photodetectors based on InAs/GaSb/AlSb superlattices**
Junkai Jiang, Faran Chang, Wenguang Zhou, Nong Li, Weiqiang Chen, Dongwei Jiang, Hongyue Hao, Guowei Wang, Donghai Wu, Yingqiang Xu and Zhi-Chuan Niu
- 038701 Hopf bifurcation and phase synchronization in memristor-coupled Hindmarsh–Rose and FitzHugh–Nagumo neurons with two time delays**
Zhan-Hong Guo, Zhi-Jun Li, Meng-Jiao Wang and Ming-Lin Ma
- 038702 Super-resolution reconstruction algorithm for terahertz imaging below diffraction limit**
Ying Wang, Feng Qi, Zi-Xu Zhang and Jin-Kuan Wang
- 038703 Effect of autaptic delay signal on spike-timing precision of single neuron**
Xuan Ma, Yaya Zhao, Yafeng Wang, Yueling Chen and Hengtong Wang
- 038704 Investigations of moiré artifacts induced by flux fluctuations in x-ray dark-field imaging**
Zhi-Li Wang, Zi-Han Chen, Yao Gu, Heng Chen and Xin Ge
- 038901 Topological phase transition in network spreading**
Fuzhong Nian and Xia Zhang

JUST FOR AUTHORS
— CHINESE PHYSICS B